CHINESE OPTICS LETTERS

Vol. 22, No. 1 | January 2024

Femtosecond laser direct written fiber Bragg gratings with narrow bandwidth and high sideband suppression

Wenping Qiu (邱文平)[1], Shuang Liu (刘 爽)[1*], Guanghua Cheng (程光华)[2], Huan Zhan (湛 欢)[3], Guodong Zhang (张国栋)[2], Guanpin Ren (任冠品)[1], Zhongrui Sun (孙中瑞)[1], and Min Zhang (张 敏)[1]

[1] Department of Applied Physics, College of Mathematics and Physics, Chengdu University of Technology, Chengdu 610059, China

[2] School of Electronics and Information, Northwestern Polytechnical University, Xi'an 710072, China

[3] Chengdu Development Center of Science and Technology of CAEP, Chengdu 610299, China

*Corresponding author: 805874667@qq.com

Received August 21, 2023 | Accepted September 6, 2023 | Posted Online January 18, 2024

Aiming for suppressing side-mode and spectrum broadening, a slit beam-shaping method and super-Gaussian apodization processing for femtosecond laser point-by-point (PbP) inscription technology of fiber Bragg gratings (FBGs) are reported here. High-quality FBGs, featuring narrow bandwidth of less than 0.3 nm, high reflectivity above 85%, low insertion loss (0.21 dB), and low cladding loss (0.82 dB), were obtained successfully. By a semi-automatic PbP inscription process, an array consisting of six FBGs, exhibiting almost no side-mode peaks with high suppression ability and narrow bandwidth, was fabricated along three independently developed single-mode fibers with an interval of 20 mm.

Keywords: femtosecond laser processing; fiber Bragg grating; slit beam shaping.
DOI: 10.3788/COL202422.010501

1. Introduction

Since Hill *et al.* proposed the first fiber Bragg grating (FBG) in 1978[1], FBG has become an indispensable part of modern optics and information technology. Traditional FBGs inscribed by UV lasers suffer from strong fiber photosensitivity dependency[2,3]. The FBG structure easily degrades at a temperature greater than 300°C. An additional hydrogen loading step also leads to low tensile strength[4]. Recently, to achieve an incredibly broad and growing range of applications such as high-temperature sensing in aerospace or oil and gas exploration, FBGs, by using femtosecond (fs) lasers, have attracted more and more attention since fs-inscribed FBGs are independent of fiber materials and exhibit an enhanced temperature-resistant performance of 1200°C[5,6].

As is well known, three mainstream fs fabrication technologies, i.e., the scanning-beam phase-mask method, the Talbot interferometer method, and the direct inscription method, have been developed for fabricating FBGs of various fiber types[7,8]. Both the scanning-beam phase-mask method and the Talbot interferometer method have not been widely adopted because of their intrinsic shortcomings. For instance, the phase-mask technology exhibits the inflexibility of wavelength-tunability and complex gratings design[5]. Both high precision and high stability are required in the fabrication process due to the extremely short path difference in experimental setup, although fs laser Talbot interferometry is more versatile in the fabrication of a wavelength-division-multiplexed (WDM) FBG array. The fs direct inscription technology does not require a phase mask[9], and the grating period, shape, and position of refractive index modulation (RIM) can be flexibly controlled; FBGs with different Bragg wavelengths and complex spectra can be obtained[10].

The fs direct inscription could be categorized into the point-by-point (PbP) method, line-by-line (LbL) method, and plane-by-plane (Pl-b-Pl) method according to the scanning trace[11–13]. For example, by a continuous core-scanning technique developed from the LbL method, high-quality FBGs, with a lower insertion loss of 0.1 dB and a higher Bragg resonance attenuation of 49 dB, were created[14]. However, fabricating a high-quality FBG takes several hours, which is not beneficial for the fabrication of FBG arrays and industrial production. Alternatively, the Pl-b-Pl method, combining the LbL scanning technology with the spherical aberration (SA) effect, has been proposed recently because it shows the advantages of high reflectivity, low loss, suppressive cladding mode coupling, and enhanced coupling strength coefficient[15]. Nevertheless, cladding mode and side-mode peaks can be easily observed in the reflection spectra of the FBGs[14,15]. Similar to the LbL method, the Pl-b-Pl method is still time-consuming, and not conducive to FBG arrays and mass production. For the previously reported PbP method, a relatively low overlap factor between the refractive index modification (RIM) region and the fiber core leads to a localized effect and therefore causes strong cladding mode loss[16]. Several methods have been proposed to suppress the

cladding mode loss, including PbP parallel-integrated inscription and beam-shaping technologies. However, these methods are not very efficient to eliminate the cladding loss or introduce additional loss. Note that the appearance of side-mode and cladding mode easily broadens the FBG spectra[17]. Moreover, compared with the Bragg resonance wavelength, the side-mode and cladding-mode peaks in the reflection spectra present comparable intensity. Owing to this additional mode peak interference, Bragg resonance wavelength and microphysical parameters (such as temperature and strain) are very difficult to be demodulated by the interrogator, especially for an FBG array or FBG string. Additionally, a large bandwidth is also disadvantageous to wavelength demodulation. To our knowledge, to accurately demodulate Bragg resonance wavelength change is a current challenge for the FBG array or string due to the above-mentioned interference, although Bragg wavelength demodulation of a single FBG is easily realized.

In this work, based on the independently fabricated single-mode fiber (SMF), FBGs with high reflectivity, low cladding mode loss, and insertion loss are successfully inscribed by a fs laser PbP technology. We applied slit beam shaping and super-Gaussian apodization processing to successfully suppress bandwidth broadening and side-mode peaks. The fabricated high-quality FBG features narrow full width at half maximum (FWHM) bandwidth of less than 0.3 nm, high resonance to side-mode peak ratio above 15 dB, and almost no side-mode peaks. By a semi-automatic inscription process, a high-quality FBG array consisting of six FBGs of the third-order and 5 mm length is successfully fabricated along a 3 m-long SMF with an interval of 20 mm and characterized by the commercial demodulator. Moreover, the corresponding FBG has excellent thermal stability, with a sensitivity of 7.91 pm/°C at 350°C.

2. Experiment

A homemade preform was drawn by a drawing tower into standard SMF (core, 9 μm; silica cladding, 125 μm; polymide cladding, 245 μm) reported in detail before elsewhere[18]. Laser exposure was conducted using a Yb:KGW medium ultrafast laser system (Pharos, Light Conversion) with a tunable repetition rate working at a wavelength of 1030 nm. The pulse duration can be easily tuned from 190 fs to 10 ps. Beam-steering optics guided the laser pulses to the workpiece, consisting of the polyimide coating SMF fiber and capillary silica tube of 600 μm diameter mounted on a three-axis air-bearing positioning system (Aerotech). The index-matching oil was applied to fill the gap between the SMF fiber and capillary silica tube so that the cylindrical lens effect caused by the surface curvature of the fiber could be eliminated. FBGs were photoinscribed by the short 1.2 ps pulses, and a repetition frequency of 1 kHz. (A pulse width of 1.2 ps imposes lower requirements on the laser source, offering a wider range of selectable energies and making beam shaping more feasible. The 1.2 ps pulse width, in comparison to pulses in the order of several hundred fs exhibits a slightly weaker nonlinear effect. This can mitigate the impact of side-mode and simultaneously enhance the efficiency of grating inscription.) The polarization of the laser has a significant impact on the grating inscription process, with the laser's polarization direction aligned parallel to the grating groove direction, resulting in the lowest energy threshold and the most precise inscription[19]. To suppress side-mode and control bandwidth, the super-Gaussian apodization region, where the focus of the incident laser was 5 μm above the center of the fiber core, was designed with a low RIM region at 0.5 mm of both the initial and end segment, respectively. In our experiment, inscription parameter optimization of FBG was not discussed here for simplification, although the inscription method was the primary focus of this work. The fabricated FBGs of the third order (grating period Λ_p = 1.55 μm) are shown in the Fig. 1(a).

According to different inscription methods, three FBGs were labeled as 1# (slit beam shaping, no super-Gaussian apodization processing), 2# (no slit beam shaping, super-Gaussian apodization processing), and 3# (slit beam shaping, super-Gaussian apodization processing). A microscope objective (50×, NA = 0.42, Mitutoyo) is used as the final focusing element. The shape of 1# and 2# samples would have an ellipse-shaped core with an aspect ratio of ≈4 : 1[20]. The slit-shaping technique has been used to ensure a circular waveguide section by our

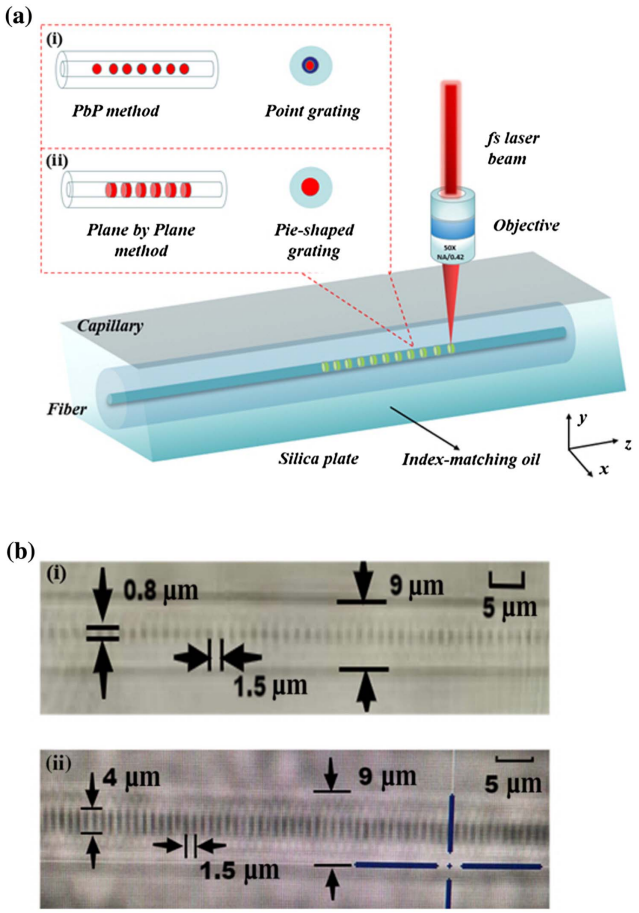

Fig. 1. (a) Schematic diagram of the experimental setup for writing FBG and FBG arrays; (b) physical images of RIM regions of varying sizes.

group before[21]. According to this, the slit before the microscope object is set to 500 μm width, and the RIM cross-sectional shape of 3# sample is round, with an aspect ratio of ≈1 : 1. Due to the difficulty in precisely controlling pulse energy after the aperture effect, the utilization of half-wave plates and polarizers to regulate pulse power and energy has enhanced the repeatability and precision of pulse energy. By employing this method, energy was measured using a high-precision power meter; the laser's pulse energy prior to beam expansion was 1.7 μJ (3# sample) and 0.5 μJ (1# and 2# samples). The pitch of the grating is decided by the moving speed of the 3D translation stage and the repetition rate of the laser. For observing the structures *in situ* in real time, an imaging transillumination system was used. *Ex situ* optical transmission and positive phase-contrast microscopy (PCM) are employed. Figure 1 shows a schematic diagram of the experimental setup for FBG inscription of the third order (grating period Λ_p = 1.55 μm). It is to be noted that, inscribed by fs laser PbP technology with no slit shaping, the length of RIM regions was 0.8 μm. By contrast, the slit-shaping method makes the RIM region in the fiber core round, and the length could be extended to 4 μm [shown in Fig. 1(b)]. Compared with the previously reported Pl-b-Pl method[22], the Pl-b-Pl method in this work, based on the slit-shaping technology and PbP method, presents a much faster inscription speed of several seconds. The increase in laser power or the reduction of the cladding mode resonance attenuation can lead to a further increase in the RIM region radius. However, extensive experimentation is required to validate the required pulse power for different fiber parameters or materials. It is evident that a 4 μm RIM region radius is not the maximum attainable value. Under the same conditions, a larger grating length implies higher reflectivity and a side-mode suppression ratio (SMSR).

As an application example, a sample with some observed sidebands, engraved 5 mm-long FBG with a resonant peak of about 1550 nm, was encapsulated into the designed ceramic module to make a temperature sensor. Thermal response of the FBG sample ceramic sensor is characterized by using the electric oven. The K-thermocouple with a TC-08 controller is used to monitor the temperature of the sample. During the heating process, the resonant behavior of the sensor is characterized and recorded by a spectrometer with a resolution of 0.1 pm and measure accuracy of ±1 pm. To calibrate the sensor and obtain the temperature sensitivity, temperature and Bragg resonant peak value are recorded at 5-min intervals.

3. Results and Discussion

In the process of grating inscribing, high-quality FBG is highly dependent on the size, ovality, and position of the fiber core[23]. It is well known that uneven distribution of the fiber refractive index profile (RIP) leads to different RIMs induced by nonlinear absorption of the fs laser at the same engraving depth, and therefore different grating RIP periods along the longitudinal direction of the fiber. In this case, the side-mode peaks and the cladding mode are easily generated by the uneven RIP

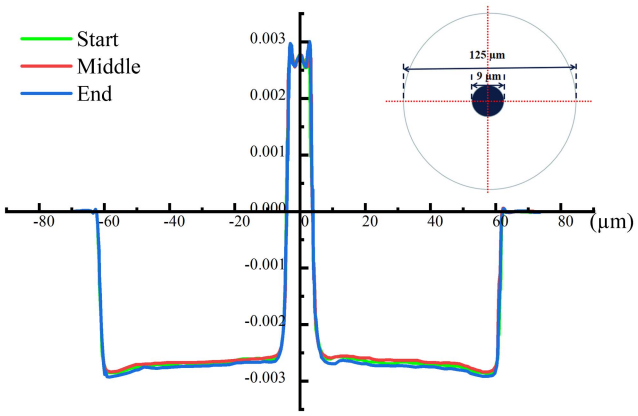

Fig. 2. RIP of the drawn 1 km-long fiber.

distribution. Figure 2 shows the RIP distribution of the initial, middle, and end segment of the drawn 1 km-long fiber. The drawn fiber is a standard SMF, with a cladding diameter of 125 μm and a core diameter of 9 μm. The numerical aperture (NA) of the core is 0.12. The propagation loss is 0.5 dB. Concentricity between the fiber core and cladding is less than 1 μm, and the noncircularity of cladding is less than 1%. To obtain a high-temperature sensor, the coating material is polyimide with a wide working temperature range of −50°C to 430°C[24]. The polyimide coating diameter is 145 μm. Note that the RIP distribution curves of the drawn fiber core in the initial, middle, and end segments are almost consistent. It ensures good period uniformity in terms of RIP and length of the inscribed FBG, thereby achieving the result of side-mode and cladding-mode suppression.

Figure 3 shows the transmission and reflection spectrum of the 3# sample with a pitch Λ of 1.5 μm and a diameter of 4 μm. The fabricated FBG of 5 mm length exhibits nearly pure resonant spectral reflection characteristics with narrow bandwidth below 0.3 nm and high side-mode suppression

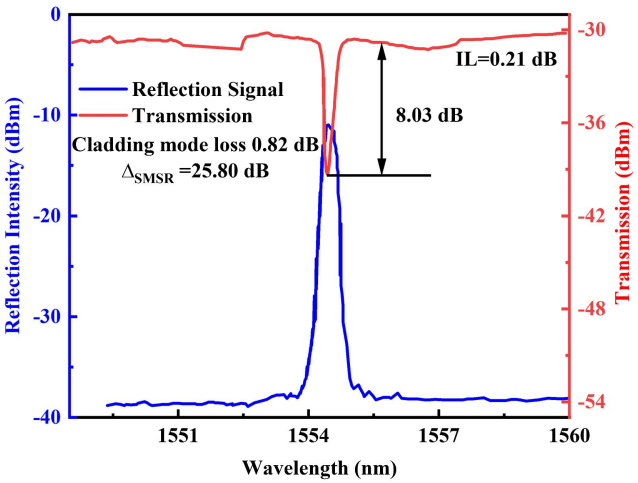

Fig. 3. Resonant spectral transmission and reflection of the 3# FBG sample at 1555 nm.

above 25 dB. It is to be noted that, according to the equation[25], the reflectivity of the FBG at the Bragg wavelength is calculated to be more than 85%. The reflectance of FBG is influenced by the polarization direction of the laser. An isotropic grating exhibits the same reflectance for identical polarized light. When the incident light direction or polarization changes, the Bragg grating demonstrates axial dependence for specific polarizations, resulting in varying reflectances[26]. Additionally, changes in the shape of the fiber due to factors such as stress can also lead to different reflectances for incident polarized light. For simplicity, in the experiment, light with the same polarization direction is used, with the incident light direction parallel to the fiber axis, to mitigate the impact of polarization direction on reflectance. As described in Fig. 3, the transmission spectrum of the 3# sample exhibits a Bragg resonance attenuation of 16.2 dB. The cladding mode resonance is controlled well; for example, the resonance attenuation at the wavelength of 1553 nm is only 0.82 dB, comparable to the counterpart (0.54 dB) reported in Ref. [27]. The RIM region is obviously less than previously reported[27]. It mainly originates from the slit-shaping technology and introduces super-Gaussian apodization region during the FBG fabrication process.

The ratio of the coupling strength coefficient to the scattering loss coefficient κ/α is a key parameter of FBG, which is a valuable index to determine the maximum achievable reflectivity of FBGs. The coupling strength coefficient κ and the scattering loss coefficient α can be expressed as $\kappa = \mathrm{In}(T_B)/(-2L)$ and $\alpha = \mathrm{In}(T_{\mathrm{IL}})/(-2L)$, where T_{IL} is the insertion loss (transmission loss measured outside the band), T_B is the Bragg resonance attenuation, and L is the length of the grating[25]. Obviously, a higher κ/α ratio will result in high reflectivity and low insertion loss. In this experiment, the insertion loss T_{IL} can be calculated as $I_L = -10\ \lg(P_{\mathrm{out}}/P_{\mathrm{in}})$, where I_L is the insertion loss, P_{out} is the output optical power, and P_{in} is the output optical power. The calculated insertion loss is extremely low, only 0.21 dB, and the Bragg resonance attenuation T_B is 8.03 dB. The coupling strength coefficient κ is 0.803, and the scattering loss coefficient α is 0.021, which can be obtained from the data. The ratio of the coupling strength coefficient to the scattering loss coefficient κ/α is 38.24, which is the much higher counterpart ($\kappa/\alpha = 17.1$) reported in Ref. [28]. It indicates the advantages of the proposed fabrication process, including slit shaping and super-Gaussian apodization process.

In order to investigate the effect of slit shaping and super-Gaussian apodization on resonant spectral characteristics, three FBG samples with different inscription processes and grating orders are fabricated. Figure 4 shows the reflection spectral response for 1#, 2#, and 3# FBG samples of 5 mm length. The 1# sample is fabricated by using slit beam shaping and no super-Gaussian apodization region. The reflection spectrum of the 1# FBG sample exhibits a third-order Bragg wavelength of 1549.55 nm, an SMSR of 16.33 dB, and an FWHM bandwidth of 0.33 nm. Intense side-mode peaks can be easily observed. It is disadvantageous for wavelength demodulation.

The 2# FBG sample, fabricated with super-Gaussian apodization region and no slit shaping, shows a reflection spectrum with

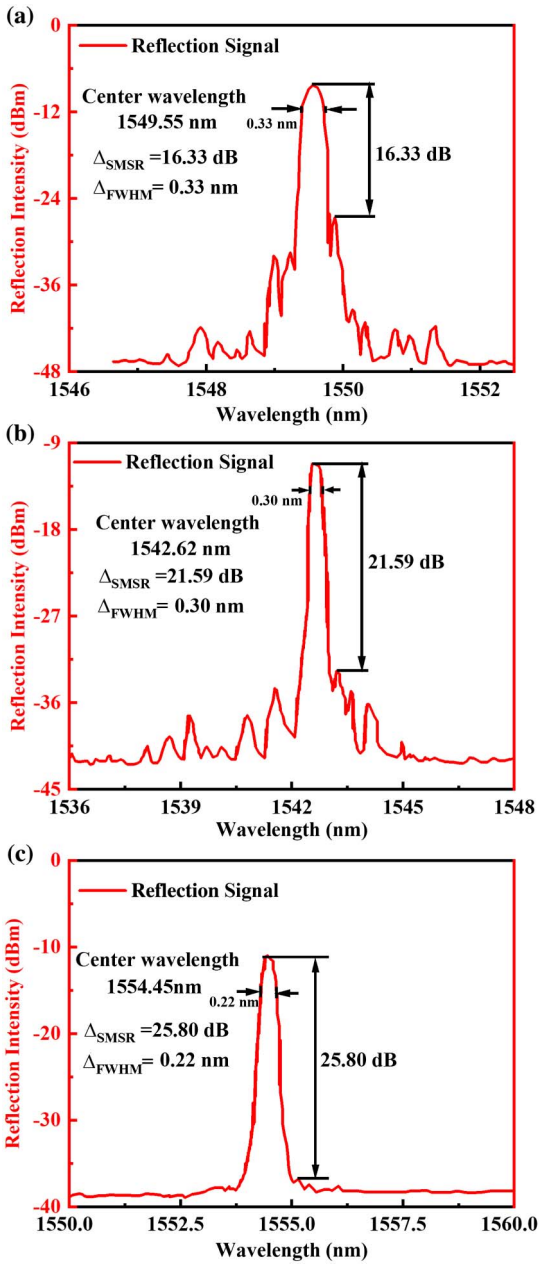

Fig. 4. Spectral characteristics of the fabricated FBG. (a) 1# sample, without slit shaping and the super-Gaussian apodization region; (b) 2# sample, with the super-Gaussian apodization region; (c) 3# sample, with a 500 μm narrow slit and super-Gaussian apodization.

a second-order Bragg wavelength of 1542.62 nm, an SMSR of 21.59 dB, and an FWHM bandwidth of 0.3 nm. Note that the 2# samples have fewer side-mode peaks compared to the 1# sample. It can be deduced that the introduced super-Gaussian apodization region is a very effective method to suppress the side mode of the Bragg resonance mode. Moreover, the super-Gaussian apodization region is efficient for spectrum-broadening suppression. By comparison, the 3# FBG sample, simultaneously inscribed by slit beam shaping and super-Gaussian apodization processing, presents a third-order Bragg

wavelength of 1554.45 nm, an SMSR of 15.31 dB, and a 3 dB bandwidth of 0.22 nm. Compared with the 1# and 2# samples, the 3# sample shows a pure response reflection spectrum with narrow bandwidth and no obvious side-mode peaks. It is very beneficial for wavelength demodulation. These results justify slit beam shaping, and the super-Gaussian apodization region contributes to avoiding the spectrum-broadening phenomenon and suppressing the side mode.

By using the above-mentioned slit beam shaping and introducing the super-Gaussian apodization region, we simultaneously design and fabricate a high-quality FBG array with no side-band mode peak and narrow bandwidth. The corresponding reflection spectral response is given in Fig. 5. The array consists of six FBGs of the third-order and of 5 mm length. The FBG array was semi-automatically fabricated in a 3 m-long SMF by using the same inscription parameters as the 3# sample. For the semi-automatic fabrication process, the SMF was fixed by a pair of fiber holders mounted on a 3D high-precision air-bearing translation stage. After the inscription of an FBG, the fiber holders are manually opened. Subsequently, a fiber feeding system, consisting of a pulley, stepper motor, and fiber spool, is used to automatically translate the fiber at 20 mm per time, i.e., the distance of 20 mm between the FBGs. The SMF was fixed, and then the reflective index oil was automatically injected into a capillary tube. To obtain auto-aligning of the laser beam focus within the fiber core center, an image-recognition algorithm was used before the FBG inscription process. The six FBG inscriptions take approximately 10 min in total.

The grating period is designed to be 1.91, 1.90, 1.89, 1.88, 1.87, and 1.86 μm, respectively. Demodulated by the commercial interrogator, the demodulation Bragg wavelengths of six FBGs are 1528.2, 1531.0, 1540.5, 1546.0, 1553.1, and 1558.2 nm, respectively. Note that all the FBGs feature high SMSRs of more than 15 dB, narrow FWHM bandwidths of less than 0.3 nm, and no obvious side-mode resonance peaks. It shows obvious advantages over an FBG array fabricated by a 266 nm fs laser

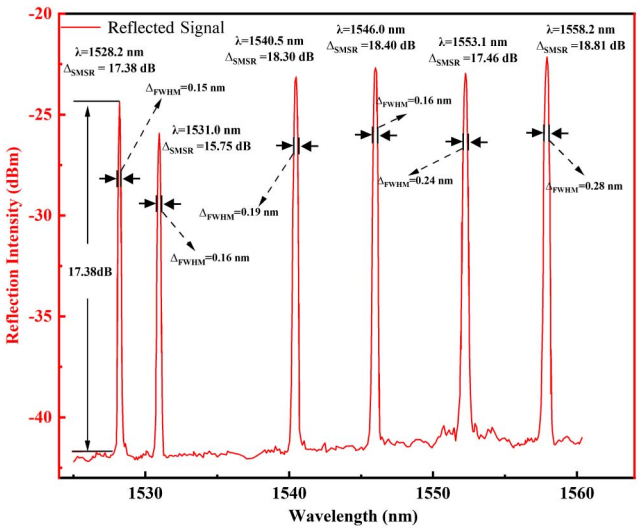

Fig. 5. Reflection response spectra of the fabricated FBG array.

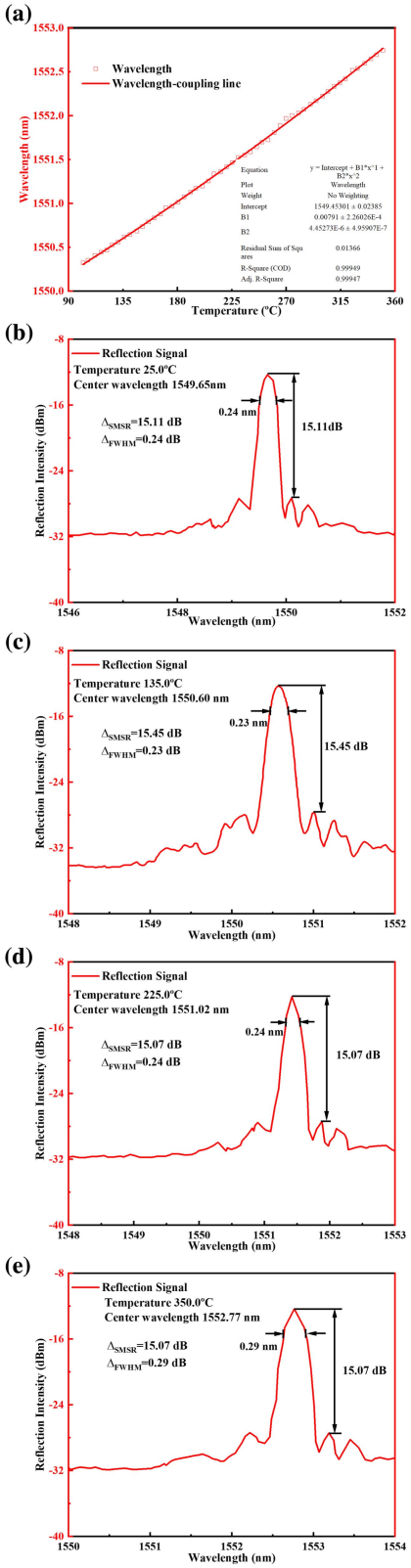

Fig. 6. (a) Relationship between the Bragg wavelength and the electric oven temperature; (b)–(e) reflection response spectra of the fabricated FBG at different temperatures (25°C, 135°C, 225°C, and 350°C).

holographic interferometry[29]. Nevertheless, the two FBGs of Bragg wavelength of 1528.2 and 1531.0 nm present relatively lower reflection peak values than the other FBGs, measuring 17.38 and 15.75 dB, which differ by 2 to 3 dB compared to the reflection peak value of 18.81 dB for the FBG with a Bragg wavelength of 1552.0 nm. The reason for this phenomenon is that some tiny bubbles existing in the immersion oil lead to the scattering of a small amount of laser beam. In addition, the FWHM bandwidth of all the FBGs is in the range of 0.15–0.28 nm, which is narrower than that of the 1# and 2# samples and advantageous for demodulating wavelength.

Furthermore, to explore the effect of temperature change on the bandwidth and side mode, an FBG sample with some low-intensity side-mode peaks, inscribed by the slit beam-shaping technology, was used for a high-temperature sensing experiment. The temperature of the electric oven increases from 100°C to 350°C, with an interval of 5°C. As shown in Fig. 6(a), the wavelength shift of the FBG sample exhibits a redshift with increasing temperature and a blueshift with decreasing temperature. The measured results are well fitted by linear fitting curves. The sensor has excellent thermal repeatability, with a sensitivity of 7.9 pm/°C. Limited by sealing glue with liquid temperature above 350°C, the sensor was not measured at the temperature above 350°C. The proposed FBG sensor has been annealed at a high temperature of 350°C for 8 h. No obvious wavelength shift was found in our experiment. As shown in Figs. 6(b)–6(e), in the sensing experiment, the FBG sensor features a high SMSR of more than 15 dB and a narrow 3 dB bandwidth of less than 0.3 nm, regardless of temperature. Note that the FWHM bandwidth presents no obvious change with the temperature increasing from 25°C to 225°C, while it slightly broadens at 350°C. This can possibly be attributed to small microcrack healing and stress relief. Moreover, with the increase of temperature from 25°C to 350°C, the Δ_{SMSR} value of the FBG exhibits almost no change, in the range of 15.07–15.45 dB. Therefore, the fabricated FBG shows excellent thermal stability, which is suitable for sensing in harsh environments.

4. Conclusion

In summary, a high-quality FBG, with almost no side-mode peak and narrow bandwidth, was inscribed and optimized in the drawn SMF by using fs laser PbP-inscription technology with the slit beam shaping and super-Gaussian apodization processing. Effects of the slit beam shaping and super-Gaussian apodization processing used for fabricating FBGs were studied. A high-quality FBG, exhibiting a narrow bandwidth of less than 0.3 nm, a high reflectivity of above 85%, a low insertion loss of 0.21 dB, and a low cladding loss of 0.82 dB, was successfully constructed. We applied the semi-automatic inscription process to fabricate a high-quality array consisting of six FBGs in a 3 m-long SMF. An FBG with the polyimide coating and some side-mode peaks was used to realize high-temperature sensing up to 350°C based on commercial demodulation. The FBG has excellent thermal stability with a sensitivity of 7.9 pm/°C at 350°C. As such, the proposed fs laser PbP technology uses a promising fabrication method for high-quality FBGs. By using this technology, multiplex FBGs used for temperature, strain, and displacement sensing will be inscribed into the SMF with the coating layer.

Acknowledgements

This work was supported by the Sichuan Provincial Natural Science Foundation (No. 23NSFSC4751).

References

1. K. O. Hill, Y. Fujii, and D. C. Johnson, "Photosensitivity in optical fiber waveguides: application to reflection filter fabrication," Appl. Phys. Lett. **32**, 647 (1978).
2. J. L. Blows, P. Hambley, and L. Poladian, "Increasing fiber photosensitivity to near-UV radiation by rare earth doping," IEEE Photon. Technol. Lett. **14**, 938 (2002).
3. P. J. Lemaire, R. M. Atkins, V. Mizrahi, *et al.*, "High pressure H_2 loading as a technique for achieving ultrahigh UV photosensitivity and thermal sensitivity in GeO_2 doped optical fibres," Electron. Lett. **29**, 1191 (1993).
4. R. Chen, J. He, X. Xu, *et al.*, "High-quality fiber Bragg gratings inscribed by femtosecond laser point-by-point technology," Micromachines **13**, 1808 (2022).
5. C. Smelser, S. Mihailov, and D. Grobnic, "Formation of type I-IR and type II-IR gratings with an ultrafast IR laser and a phase mask," Opt. Express **13**, 5377 (2005).
6. Y. Li, M. Yang, C. Liao, *et al.*, "Prestressed fiber Bragg grating with high temperature stability," J. Lightwave Technol. **29**, 1555 (2011).
7. K. Oi, F. Barnier, and M. Obara, "Fabrication of fiber Bragg grating by femtosecond laser interferometry," in *14th Annual Meeting of the IEEE Lasers and Electro-Optics Society* (2001), p. 776.
8. S. J. Mihailov, C. W. Smelser, P. Lu, *et al.*, "Fiber Bragg gratings made with a phase mask and 800-nm femtosecond radiation," Opt. Lett. **28**, 995 (2003).
9. A. Martinez, M. Dubov, I. Khrushchev, *et al.*, "Direct writing of fibre Bragg gratings by femtosecond laser," Electron. Lett. **40**, 1170 (2004).
10. B. Xu, J. He, B. Du, *et al.*, "Femtosecond laser point-by-point inscription of an ultra-weak fiber Bragg grating array for distributed high-temperature sensing," Opt. Express **29**, 32615 (2021).
11. Y. Kondo, K. Nouchi, T. Mitsuyu, *et al.*, "Fabrication of long-period fiber gratings by focused irradiation of infrared femtosecond laser pulses," Opt. Lett. **24**, 646 (1999).
12. K. Zhou, M. Dubov, C. Mou, *et al.*, "Line-by-line fiber Bragg grating made by femtosecond laser," IEEE Photon. Technol. Lett. **22**, 1190 (2010).
13. A. Theodosiou, J. Aubrecht, P. Peterka, *et al.*, "Er/Yb double-clad fiber laser with fs-laser inscribed plane-by-plane chirped FBG laser mirrors," IEEE Photon. Technol. Lett. **31**, 409 (2019).
14. R. J. Williams, R. G. Kramer, S. Nolte, *et al.*, "Femtosecond direct-writing of low-loss fiber Bragg gratings using a continuous core-scanning technique," Opt. Lett. **38**, 1918 (2013).
15. B. Huang, Z. Xu, and X. Shu, "Dual interference effects in a line-by-line inscribed fiber Bragg grating," Opt. Lett. **45**, 2950 (2020).
16. W. He and L. Zhu, "A femtosecond laser inscribed fiber Bragg grating as a refractive index and temperature sensor based on side-polished method," Mod. Phys. Lett. B **34**, 2050296 (2020).
17. J. He, B. Xu, X. Xu, *et al.*, "Review of femtosecond-laser-inscribed fiber Bragg gratings: fabrication technologies and sensing applications," Photonic Sens. **11**, 203 (2021).
18. S. Liu, H. Zhan, K. Peng, *et al.*, "Yb-doped triple-cladding laser fiber fabricated by chelate precursor doping technique," in *Asia Communications and Photonics Conference (ACP)* (2018), p. 1.
19. J.-Q. Liang, G.-S. Zhou, and M. Mohebi, "The relationship between laser polarization orientation and the energy absorption and damage threshold of the grating," Acta Opt. Sin. **5**, 9 (1989).

20. M. Ams, G. Marshall, D. Spence, *et al.*, "Slit beam shaping method for femtosecond laser direct-write fabrication of symmetric waveguides in bulk glasses," Opt. Express **13**, 5676 (2005).
21. G. Zhang, G. Cheng, M. Bhuyan, *et al.*, "Efficient point-by-point Bragg gratings fabricated in embedded laser-written silica waveguides using ultrafast Bessel beams," Opt. Lett. **43**, 2161 (2018).
22. A. Ioannou, A. Theodosiou, C. Caucheteur, *et al.*, "Direct writing of plane-by-plane tilted fiber Bragg gratings using a femtosecond laser," Opt. Lett. **42**, 5198 (2017).
23. S. Liu, R. Zhu, J. Wang, *et al.*, "3 kW 20/400 Yb-doped aluminophosphosilicate fiber with high stability," IEEE Photonics J. **10**, 1503408 (2018).
24. M. I. Bulatov and A. A. Shatsov, "Strength and fracture resistance of quartz fibers with polyimide coatings," Russ. J. Non-Ferr. Met. **62**, 756 (2021).
25. R. J. Williams, N. Jovanovic, G. D. Marshall, *et al.*, "Optimizing the net reflectivity of point-by-point fiber Bragg gratings: the role of scattering loss," Opt. Express **20**, 13451 (2012).
26. M. P. Araújo, S. De Leo, and G. G. Maia, "Axial dependence of optical weak measurements in the critical region," J. Opt. **17**, 035608 (2015).
27. J. Wu, X. Xu, C. Liao, *et al.*, "Optimized femtosecond laser direct-written fiber Bragg gratings with high reflectivity and low loss," Opt. Express **31**, 3831 (2023).
28. X. Xu, J. He, J. He, *et al.*, "Slit beam shaping for femtosecond laser point-by-point inscription of high-quality fiber Bragg gratings," J. Lightwave Technol. **39**, 5142 (2021).
29. A. Saliminia and R. Vallée, "Fiber Bragg grating inscription based on optical filamentation of UV femtosecond laser pulses," Opt. Commun. **324**, 245 (2014).